Progress In Electromagnetics Research, Vol. 150, 1–12, 2015

An Adaptive Path Loss Channel Model for Wave Propagation in Multilayer Transmission Medium

Mohammad H. Ramezani[1, *], Victoria Blanes-Vidal[2], and Esmaeil S. Nadimi[1]

Abstract—Advances in micro robots in non-invasive medicine have enabled physicians to perform diagnostic and therapeutic procedures with higher resolution and lower risk than before. However, navigation and precise localisation of such micro robots inside human body still remains a challenge. This is mostly due to the 1) lack of precise communication channel models, 2) inhomogeneity of the propagation medium and 3) non-geometric boundaries of the tissues morphometric parameters. In this study, we derive novel intra-body path loss channel models for wave propagation in wireless capsule endoscopy, i.e., propagation through the gastrointestinal tract and the abdominal wall. We formulate an adaptive attenuation parameter as a function of permittivity, conductivity and the thickness of various layers between the transmitter and the receiver. The standard deviation of modelling error of the path loss using our adaptive channel model is smaller than 50% of that of existing channel models. We further analyse the sensitivity of the path loss model to the variations of thickness of different abdominal wall layers. We finally show that the thickness of the fat layer has the greatest influence on the total attenuation parameter of the path loss model and therefore, we modify our adaptive model accordingly.

1. INTRODUCTION

Recent advances in the development of micro robots for non-invasive medical procedures have enabled physicians to perform examinations with higher reliability and less pain than before. As an example, wireless capsule endoscopy for gastrointestinal (GI) tract disease monitoring is a powerful diagnostic tool that offers functional information as the capsule moves passively through the GI tract. It yields greater magnification than traditional endoscopy while providing excellent resolution. However, even with these technological advances, certain limitations due to the lack of precise spatial information still remain in the navigation and localisation of the capsule [1].

Since capsule localisation is directly based on the estimation of the distance between the capsule and a set of receivers placed outside the body, enhancing the estimation of this distance results in localisation improvement. Various methods have been introduced for distance estimation, such as magnetic field intensity [2, 3], time of arrival (TOA) [4] and the received signal strength indicator (RSSI) [5, 6]. The magnetic-based and the TOA-based solutions have received less attention than the RSSI-based solutions due to the fact that the first ones enlarge the capsule (since they need a permanent or a transient magnet) while the second ones require precise synchronisation between the transmitter and the receiver, at the cost of extra synchronous clocks. The RSSI-based solutions, on the other hand, have been more attractive for many researchers due to their simplicity and low cost, even though they suffer from low precision and high dependency on the propagation medium properties. Localisation of an endoscopic capsule for GI tract monitoring with an error margin ranging from 3 to 10 cm is acceptable.

Received 7 March 2015, Accepted 3 April 2015, Scheduled 3 April 2015

* Corresponding author: Mohammad H. Ramezani (ramezani@mmmi.sdu.dk).

[1] Applied Statistical Signal Processing Group (πSeG), Maersk Mc-Kinney Moller Institute, Faculty of Engineering, University of Southern Denmark, Denmark. [2] Department of Chemical engineering, Biotechnology and Environmental Engineering, Faculty of Engineering, University of Southern Denmark, Denmark.

Variations in the electromagnetic properties (i.e., permittivity ϵ' and conductivity σ) of the transmission medium directly affect the precision of the model describing the communication channel between the transmitter (e.g., endoscopic capsule) and the receiver. Path loss channel models of human body as a function of distance with constant attenuation coefficient have been modelled under different scenarios in body area networking, such as around the body [7–9], on the body [10, 11] and inside the body [2, 12–16]. In these studies, the human body was assumed as a homogeneous transmission medium. However, human body is an inhomogeneous transmission medium due to the presence of different tissues (such as fat, muscle and lumen) with different ϵ' and σ and physical thicknesses, in addition to enhanced shadowing, multi-path fading and reflection. Furthermore, some studies simulated the wave propagation inside human body using a Finite-Difference-Time-Domain (FDTD) based numerical software (SEMCAD) [7, 17–19]. Other more rigorous studies considered the variation in model parameters with human age [9] and the sensitivity of the path loss model to the dielectric parameters of different tissues [10]. The analysis of the stochastic nature of the uncertainties has been conducted in [9, 11, 20, 21]. In [4], variations of the attenuation coefficient for different genders, heights, and other individual properties (as those described in [7, 15]) have been investigated. A probability distribution for path loss exponent including the effect of inhomogeneity in tissues ϵ' was derived in [22]. All these studies and our future studies involving the use of animal subjects or humans have been carried out in accordance with the EU Directive 2010/63/EU for animal and human experiments.

In addition to the inhomogeneity of the human body, the differences in electromagnetic properties (ϵ' and σ) among the abdominal wall layers affect the path loss channel model. For instance, ϵ' and σ of muscle are approximately five and ten times larger than those of fat, respectively [23]. In addition, inter-individual variability and non-geometric boundaries of the tissues morphometric parameters call for a more precise path loss model with adaptive attenuation coefficient.

The first objective of this study is to investigate the effect of the thickness of different abdominal wall layers on the path loss model between the transmitter and the receivers. The impact of the variations of electromagnetic properties of the abdominal wall layers on the path loss model has been well studied in the literature. This study provides information on the effect of the variations of the thickness of the abdominal wall layers on the path loss model and the accuracy of distance estimation. We derive a multilayer channel model (hereafter referred to as "MultiLayer Model") of the transmission medium and study the effect of thickness variations on the models performance. The second objective of this study is to derive an adaptive model of the path loss as a function of the thickness of the abdominal wall layers (referred to as "Adaptive Model") where the medium is considered as a single layer model. In this model, we define an adaptive attenuation parameter α dependent on ϵ', σ and the thickness of different layers. We propose two methods to estimate α, one based on the measurements of the total reflected power and another using weighted means of ϵ', σ and the thickness of the layers. We further show that, in spite of the inequality of distances between the transmitter and various receivers on the body, this model significantly improves the path loss estimation. Finally, we derive another single layer-based channel model of the medium in which the attenuation parameter in the path loss model is the solution to an optimisation problem over different layer thicknesses. This model is referred to as the "Fixed-Optimised-Model". Using Monte Carlo simulation, the performance of the Adaptive Model and the Fixed-Optimised-Model are then compared with that of the MultiLayer-model. The main shortcoming of the MultiLayer Model, Adaptive-Model and the Fixed-Optimised-Model is their dependency on the values of the thickness of different layers. We therefore derive a novel adaptive model, referred to as "Adaptive Model 2" in which only the thickness of the fat layer is required and the thickness of the other layers are set to their nominal values.

2. MULTILAYER CHANNEL MODELLING

In this section, the transmission medium (i.e., abdominal wall) is modelled as a multilayer medium and we derived the time-average power at each location inside the medium and the total reflected power as a function of layers electromagnetic properties.

2.1. Time-Average Power

In this study, we model the abdominal wall as a multilayer medium composed of homogenous slabs [24–26]. Figure 1(a) shows the multilayer structure of the abdominal wall and Figure 1(b) describes the propagation of waves in a lossy multilayer structure. Considering electric (E) and magnetic (H) fields as being linearly polarised along x and y direction, respectively, and propagating along the z direction, $E(z)$ and $H(z)$ at each location along the z axis can be computed as a function of forward and backward electric fields ($E_+(z)$, $E_-(z)$) as follows:

$$\begin{cases} E(z) = E_+(z) + E_-(z) \\ H(z) = \dfrac{1}{\eta(z)}(E_+(z) - E_-(z)) \end{cases} \tag{1}$$

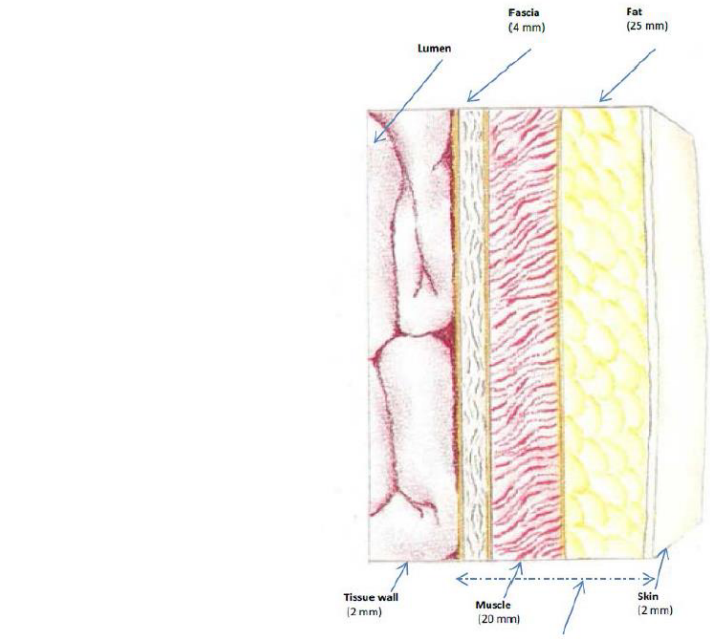

(a)

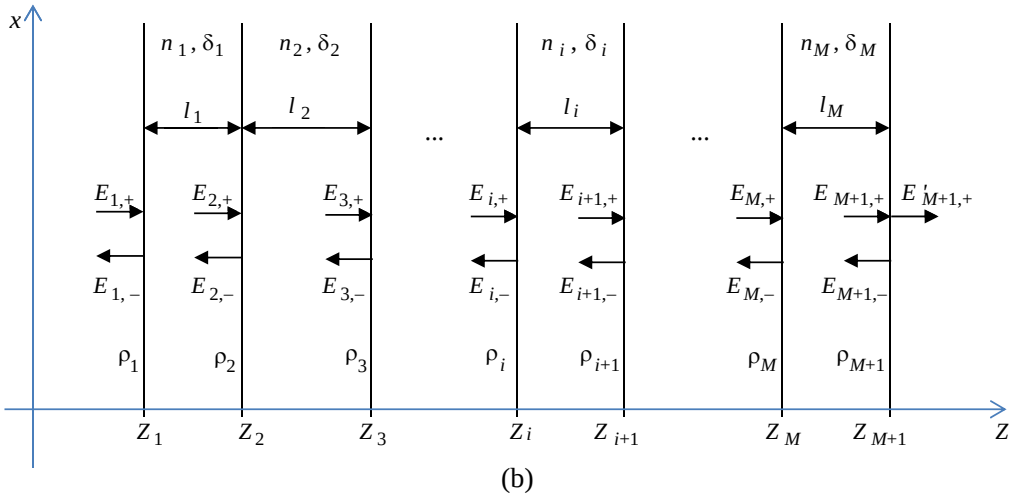

(b)

Figure 1. (a) Multilayer structure of the abdominal wall. (b) Propagation of electric field throughout a multilayer medium.

where $\eta(z)$ is the characteristic impedance of the nonmagnetic material described as:

$$\eta(z) = \frac{1}{n(z)}\eta_0 \tag{2}$$

η_0 is the characteristic impedance of the vacuum and n the refractive index of the material. For a lossy material, n is a function of permittivity (ϵ') and conductivity (σ) as follows:

$$n = \sqrt{\epsilon_r} = \sqrt{\epsilon' - j\epsilon''} = \sqrt{\epsilon' - \frac{j\sigma}{\epsilon_0\omega}} \tag{3}$$

In Eq. (3), ϵ_0 is the permittivity of vacuum and ω the angular frequency. Now, using the matching and propagation matrices for transverse fields, the layer recursions for multiple dielectric slabs can be derived. The layer recursions represent the electric fields in each location along the z axis ($E_{\pm}(z)$) as a function of incident electric field (Please refer to Appendix A). Substituting $E_{\pm}(z)$ in (1), the time-average power for this linearly polarised plane wave can be calculated using the pointing vector as follows:

$$P_{av}(z) = P_{r-ML}(z) = \frac{1}{2}\mathrm{Re}\left(E(z)H^*(z)\right) \tag{4}$$

2.2. Total Reflected Power

An incident field to a multilayer medium results in transmitted power, reflected power and power loss depending on the characteristics of the layers, i.e., thickness, ϵ' and σ. Having access to the measurements of $E_{i,-}$ and given that the reflected coefficient Γ_i at each interface i is the ratio of $E_{i,-}$ to $E_{i,+}$ in that interface i, the relationship between $E_{i,-}$ and the medium parameters are derived as follows:

$$\Gamma_i = \frac{E_{i,-}}{E_{i,+}} \tag{5}$$

Furthermore, the first scattering parameter, s_{11}, is the ratio of the power parameters b_1 and a_1:

$$s_{11} = \frac{b_1}{a_1} \tag{6}$$

where in condition that the characteristic impedance of the left dielectric medium, i.e., η_a, is real (which is a realistic assumption given that the left dielectric layer is part of the measuring probe), b_1 and a_1 are as follows:

$$b_1 = \frac{E_{1,-}}{\sqrt{\eta_a}}, \quad a_1 = \frac{E_{1,+}}{\sqrt{\eta_a}} \tag{7}$$

Substituting (7) into (6) yields:

$$s_{11} = \frac{E_{1,-}}{E_{1,+}} = \Gamma_1 \tag{8}$$

Given the reflected coefficient Γ_1 of the first interface, the input impedance Z_1 can be calculated using the following equation:

$$Z_1 = \eta_a \frac{1+\Gamma_1}{1-\Gamma_1} \tag{9}$$

Since the input impedance of an infinitely large and homogeneous medium is equal to the characteristic impedance of that medium, the value of Z_1 for a multilayer medium can be interpreted as the effective characteristic impedance of the whole medium:

$$Z_1 = \eta_{eff} \tag{10}$$

using (2) and (3), the effective value for permittivity (ϵ'_{eff}) and conductivity (σ_{eff}) of the whole medium can be calculated as follows:

$$Z_1 = \eta_0 \left(\epsilon'_{eff} + \frac{j\sigma_{eff}}{\epsilon_0\omega}\right)^{-\frac{1}{2}} \tag{11}$$

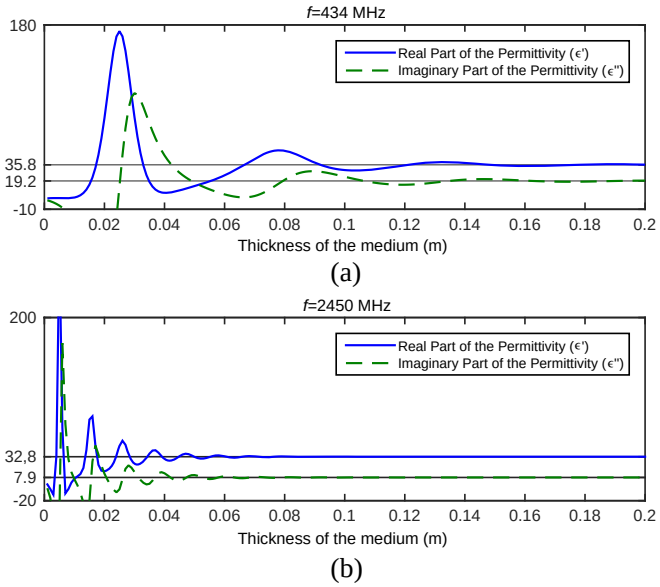

Figure 2. Estimated permittivity from reflected power. (a) $f = 434\,\text{MHz}$. (b) $f = 2450\,\text{MHz}$.

The assumption of infinitely largeness of the medium under test poses a constraint on the minimum thickness of the material needed to be considered semi-infinite. This minimum thickness depends on the ϵ' of the material and the angular frequency of the propagated wave. Estimated values of ϵ'_{eff} of the abdominal wall of a pig with the nominal values of ϵ' and σ at 434 MHz and 2.4 GHz are presented in Figure 2. It can be readily inferred that the sensitivity of ϵ'_{eff} and therefore the reflected power to the variations of the layers' thickness when below the minimum thickness (20 cm at 434 MHz and 7 cm at 2.45 GHz), is significant.

3. ADAPTIVE PATH LOSS MODEL

In this section, we derive a general model for the received power (path loss) as a function of the attenuation parameter and distance measurements between the transmitter and the receiver in a single layer medium. We further extend our model to a multilayer medium with M layers and derive the new total attenuation parameter based on the physical and electromagnetic properties of the layers.

3.1. Path Loss: Single Layer Medium

For a lossy medium with relative permittivity ϵ' and conductivity σ, the propagation of E_- and E_+ are presented by the following equation [27]:

$$E_{\pm}(z) = E_{0\pm} e^{\mp \gamma z} \tag{12}$$

where γ is the complex propagation constant defined as below:

$$\gamma = \alpha + j\beta = j\omega\sqrt{\mu\epsilon_0\epsilon'}\sqrt{1 - \frac{\sigma}{j\omega\epsilon_0\epsilon'}} \tag{13}$$

in which α and β are attenuation and phase constants, respectively. Separating the amplitude and the phase of the E field elements as:

$$\begin{cases} E_+(z) = E_{0+}\, e^{-\alpha z} e^{-j\beta z} \\ E_-(z) = E_{0-}\, e^{\alpha z} e^{j\beta z} \end{cases} \tag{14}$$

and assuming a dominant value for the amplitude of the forward term, i.e.:

$$E_{0+}\, e^{-\alpha z} \gg E_{0-} e^{\alpha z} \tag{15}$$

The time-average power can be simplified as follows:

$$P_{av}(z) \approx \frac{1}{2\mathrm{Re}(\eta)} \left|E_{+}(z)\right|^2 = \frac{1}{2\mathrm{Re}(\eta)} e^{-2\alpha z} \tag{16}$$

The path loss (dB) has the following form:

$$PL_{\mathrm{dB}} = 10\ \log_{10} P_{av}(d_0) - 10 \log_{10} P_{av}(d) \approx -20 \log_{10} e^{-\alpha d} \tag{17}$$

where d is the distance between the transmitter and the receiver and the power in d_0 is set to 0 dB.

3.2. Attenuation Parameter: Multilayer Medium

In Eq. (17), the attenuation parameter α represents the rate of path loss with respect to d. In the case of a single layer medium, α is a function of ϵ' and σ of the medium (Eq. (13)), while in a multilayer medium, it depends on ϵ', σ and the thickness of all layers. In order to estimate α in the multilayer case, the whole medium can be considered as a single layer medium with effective values for ϵ' and σ. These values can either be estimated by measuring s_{11} (using Eq. (18)) or as in this study, by deriving the weighted average of ϵ' and σ of all layers [28], i.e.:

$$\bar{\epsilon}' = \frac{\sum_{i=1}^{M} \epsilon_i' l_i}{\sum_{i=1}^{M} l_i}, \quad \bar{\sigma} = \frac{\sum_{i=1}^{M} \sigma_i l_i}{\sum_{i=1}^{M} l_i} \tag{18}$$

where l_i, ϵ_i' and σ_i are the thickness, permittivity and conductivity of the ith layer, respectively. Consequently, the attenuation parameter for the multilayer medium α_{ad} can be estimated as follows:

$$\alpha_{ad} = \mathrm{Re}\left(j\omega \sqrt{\mu\epsilon_0 \bar{\epsilon}' \left(1 - \frac{\bar{\sigma}}{j\omega\epsilon_0\, \bar{\epsilon}'}\right)} \right) \tag{19}$$

Since α_{ad} is a function of the thicknesses of the layers, the model varies in an adaptive manner and we will refer to this model as the Adaptive Model.

4. SIMULATION RESULTS

In this section, we present the performance of several models for the propagation of EM wave through the abdominal wall. The structure of these models are presented in Figure 3. The first model, referred to as Multilayer Model, is based on the structure presented in Figure 1(b) and is the most accurate model as the precise values of ϵ', σ and l_i of each layer is required. The second model, referred to as the Fixed-Optimised-Model, is the solution to an optimisation problem minimising RMSE of the received powers after 20,000 Monte Carlo simulations. The third model is the adaptive model presented in the previous section by Eqs. (24)–(26), (i.e., Adaptive Model). The forth model (Adaptive Model 2) is an applied realisation of the Adaptive Model and will be derived in the following section. We assumed Gaussian distribution over the thickness of all layers with mean and standard deviations equal to the nominal values and 20% of the nominal values of layer thickness, respectively.

Furthermore, the sensitivity analysis of the received power to the variations of tissue properties around their nominal value is investigated.

4.1. Multilayer Simulation and Sensitivity Analysis

During a capsule endoscopy, the transmission interface between the transmitter and the receivers is composed of lumen, the wall of intestine, fascia, muscle, fat and skin with thickness nominal values of approximately 3, 2, 4, 20, 25 and 2 mm, respectively [29]. Figure 4 shows the trend of power loss through the abdominal wall with vertical grids indicating the interfaces between different layers. It can be readily inferred from the figure that the rate of power loss variations vary significantly from one

layer to another one. As instance, path loss in the fat layer is much smaller than that of a thinner muscle layer (1.5 dB compared to 3.3 dB). This difference is due to the large difference between the electromagnetic characteristics of the two layers since ϵ' and σ of muscle are almost 5 and 10 times larger than those of fat, respectively. As a result, the ratio of the layers thickness has an impact on the path loss channel model. It can be inferred from Figure 3 that the slope of the curve (received power vs. distance) throughout the medium in the Adaptive Model is not constant indicating that this model estimates different attenuation rates for the received power at different layers.

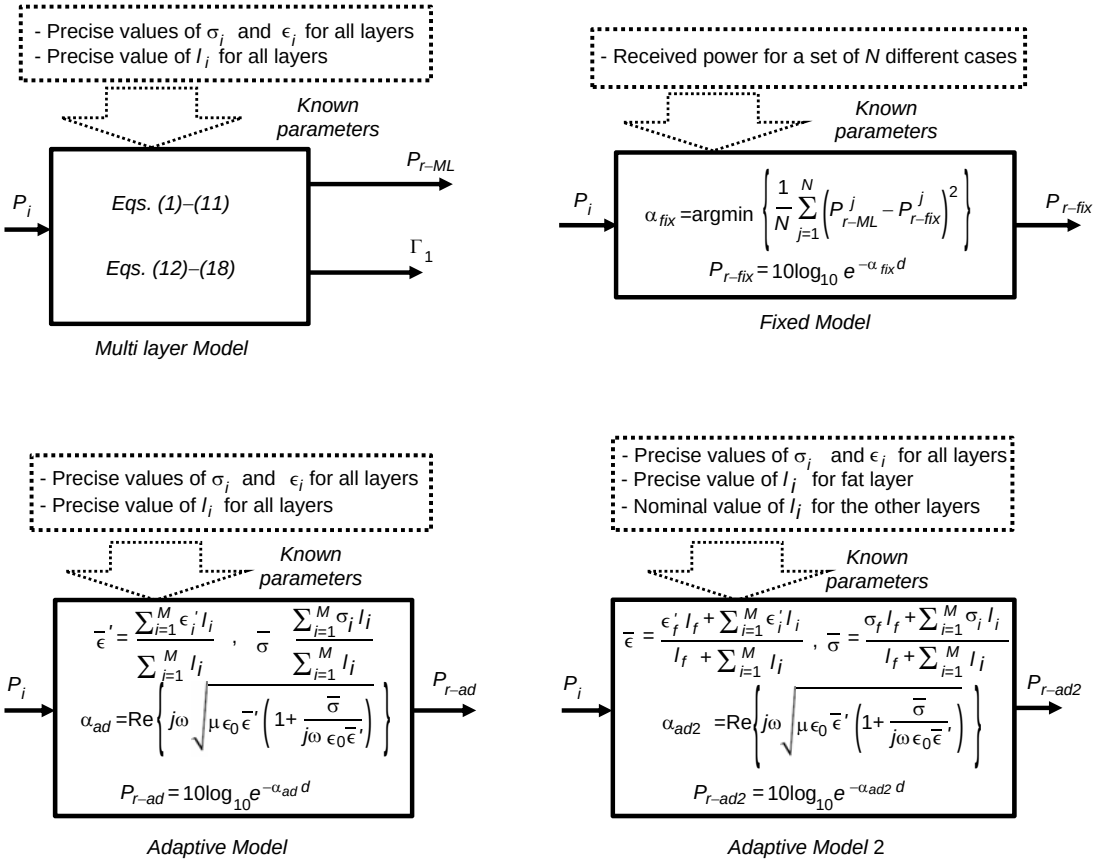

Figure 3. Structure of multilayer, fixed, Adaptive Model and Adaptive Model 2.

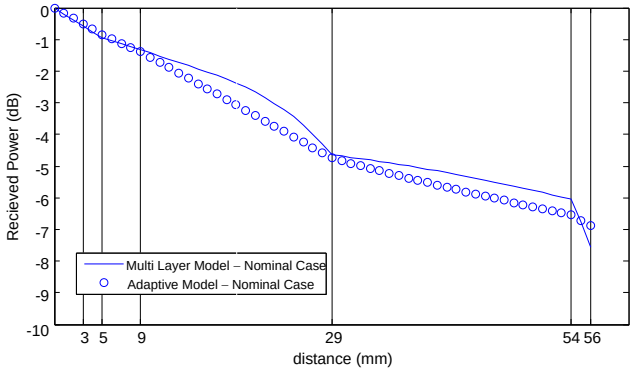

Figure 4. Trend of power attenuation in the multilayer model of abdominal medium.

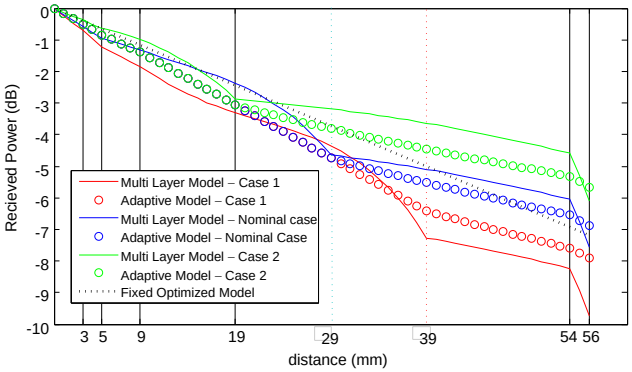

Figure 5. Power attenuation in abdominal wall layers for three different fat to muscle thickness ratios. Case-1: $\frac{15}{30}$, Nominal Case: $\frac{25}{20}$, Case-2: $\frac{35}{10}$.

In order to investigate the effect of the variations of thickness ratio of the different layers (sensitivity analysis), the received power estimated by the Multilayer Model and Adaptive Model in Figure 4 with nominal values of tissue properties are compared with two other cases. These two cases address different fat to muscle thickness ratios while keeping the distance between the transmitter and the receiver as nominal (56 mm). In Case-1 the ratio of fat to muscle thickness is set to $\frac{15}{30}$ while in Case-2 the ratio is $\frac{35}{10}$. Nominal Case is referred to the nominal value of the ratio ($\frac{25}{20}$). The received power vs. distance for Case-1, Case-2, Nominal Case and that of the Fixed-Optimised Model are presented in Figure 5. It can be seen that, although the Adaptive Model cannot precisely model the path loss in different abdominal wall layers, its performance is still more accurate than that of the Fixed-Optimised Model due to the inclusion of the thickness of the layers.

4.2. Statistical Analysis of the Path Loss Models

In order to investigate the effect of thickness variation of the layers in the aforementioned scenarios, we assume Gaussian distribution over the thickness of all layers with mean and standard deviations equal to the nominal values and 20% of the nominal values of layer thickness, respectively. The simulations are performed $20,000$ times using Monte Carlo method and the received powers in different scenarios are calculated using the multilayer model. The errors, i.e., e_{ad} and e_{fix} of the single layer-based models (Adaptive-Model and Fixed-Optimised-Model) are as follows:

$$\begin{aligned} &\text{Adaptive Model:} \quad P_{r-ad}\,(\text{dB}) = 10\log_{10} e^{-\alpha_{ad}\,d}, \quad e_{ad} = P_{r-ML} - P_{r-ad} \\ &\text{Fixed Model:} \quad\;\; P_{r-fix}\,(\text{dB}) = 10\log_{10} e^{-\alpha_{fix}\,d}, \quad e_{fix} = P_{r-ML} - P_{r-fix} \end{aligned} \tag{20}$$

where α_{fix} is the optimal solution of the optimisation problem minimising RMSE among all simulated conditions. The value of α_{ad} depends on ϵ' and σ (Eqs. (18), (19)) which varies at each simulation. The simulation results are shown in Figure 6 in which the distribution of errors of adaptive and fixed models are presented. As it can be seen, the modelling error of α_{ad} (0.33) is smaller than half of that of the fixed model (0.71).

The requirement of having access to all layer thicknesses in the adaptive model is the main disadvantage of such a model. To address this shortcoming, we propose a solution that takes only the thickness of the fat layer into account. It should be noted that Eq. (18) is a weighted average over all layers, and therefore the thickest layers (i.e., muscle and fat) have more impact on the final results than the thinner ones. Therefore, given that ϵ' and σ of fat are significantly different from those of other tissues, variations of the fat thickness have the most influence on the effective values. Furthermore, the thickness of the fat layer can be estimated using straightforward medical tests. Measurement of the thickness of the fat layer around the abdominal wall can be readily carried out. Consequently, the adaptive model is re-run assuming that only the fat thickness is known, while the value of other thicknesses are set to their nominal values. The simulation results show that although the variance

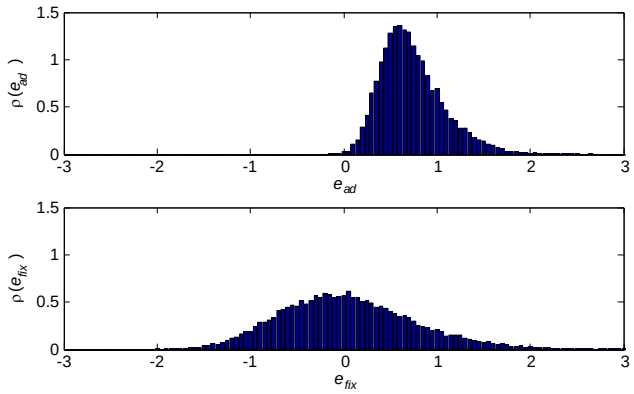

Figure 6. Density of modeling error for the adaptive and fixed models.

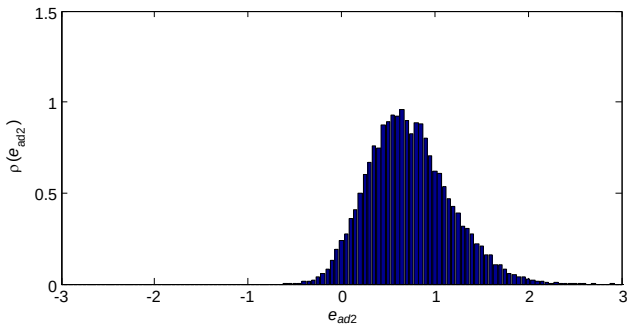

Figure 7. Density of modelling error for the second adaptive mod.

of the modelling error (0.41 in this case) is larger than that of the previous adaptive model, it is still smaller than the fixed model. Figure 7 shows the density of the modelling error for the new adaptive model.

4.3. Statistical Analysis of the Localisation Error

In order to investigate the performance of the proposed adaptive path loss model, localisation of an unknown transmitter inside the large intestine using eight receivers (anchors) outside the body is simulated. In this simulation, the transmitter node is located at the origin and the receivers are placed in fixed azimuth and elevation directions (with varying distances) with respect to the transmitter as follows:

$$\begin{aligned}[\theta_1\ \theta_2\ \theta_3\ \theta_4\ \theta_5\ \theta_6\ \theta_7\ \theta_8] &= [45\ 0\ -45\ 90\ 0\ -90\ 135\ -135] \\ [\phi_1\ \phi_2\ \phi_3\ \phi_4\ \phi_5\ \phi_6\ \phi_7\ \phi_8] &= [45\ 45\ 45\ 45\ 90\ 45\ 45\ 45]\end{aligned} \tag{21}$$

The distances between the transmitter and the receivers depend on the thicknesses of the layers in between which differ for the different sensors. In the simulations performed for 2500 different bodies based on the Monte Carlo method, the thicknesses of the layers between the transmitter and each receiver are considered Gaussian random variables with nominal mean value and 20% standard deviation. Furthermore, the thickness of lumen, the wall of intestine and skin are assumed to be constant values for all the 8 receivers. The received power in each receiver is computed using multilayer model while the distance between the transmitter and each receiver is estimated using the Fixed-Optimised Model and Adaptive Model 2 as follows:

$$\begin{aligned}\hat{d}_{ad-2} &= \frac{P_{r-ML}\,(\mathrm{dB}) - \beta}{\alpha'_{ad-2}}; \quad \alpha'_{ad-2} = \frac{20\ \alpha_{ad-2}}{ln10}, \quad \beta = E\{e_{ad-2}\} \\ \hat{d}_{fix} &= \frac{P_{r-ML}\,(\mathrm{dB})}{\alpha'_{fix}}; \quad \alpha'_{fix} = \frac{20\alpha_{fix}}{\ln 10}\end{aligned} \tag{22}$$

Applying the multi-lateration algorithm [30], the location of the transmiter can be estimated using the location of the 8 receivers:

$$\begin{bmatrix}\hat{x} \\ \hat{y} \\ \hat{z}\end{bmatrix} = \left(A^T A\right)^{-1} A^T B \tag{23}$$

where:

$$A = 2\begin{bmatrix} x_1 - x_8 & y_1 - y_8 & z_1 - z_8 \\ x_2 - x_8 & y_2 - y_8 & z_2 - z_8 \\ \vdots & \vdots & \vdots \\ x_7 - x_8 & y_7 - y_8 & z_7 - z_8 \end{bmatrix}, \quad B = \begin{bmatrix} \hat{d}_1^2 - \hat{d}_8^2 \\ \hat{d}_2^2 - \hat{d}_8^2 \\ \vdots \\ \hat{d}_7^2 - \hat{d}_8^2 \end{bmatrix} + \begin{bmatrix} \left(x_8^2 + y_8^2 + z_8^2\right) - \left(x_1^2 + y_1^2 + z_1^2\right) \\ \left(x_8^2 + y_8^2 + z_8^2\right) - \left(x_2^2 + y_2^2 + z_2^2\right) \\ \vdots \\ \left(x_8^2 + y_8^2 + z_8^2\right) - \left(x_7^2 + y_7^2 + z_7^2\right) \end{bmatrix} \tag{24}$$

in which (x_i, y_i, z_i) is the coordinate of ith receiver sensor. The simulation results show that the localisation RMSE using the Fixed-Optimised Model and Adaptive Model 2 are 17.8 mm and 10.9 mm, respectively. Assuming that the standard deviation of the variation of layers thickness is 10 % of their nominal value, this localisation error is reduced to 8.9 mm and 5.9 mm, respectively.

5. DISCUSSION AND CONCLUDING REMARKS

The impact of the variations of ϵ' and σ of the abdominal wall layers on the path loss model has been studied in the literature. Our study provides information on the effect of the variations of the thickness of the abdominal wall layers on the attenuation parameter of the path loss model and the accuracy of distance estimation. We derived two single layer-based models (i.e., Fixed-Optimised Model and Adaptive Model) to estimate the distance between the transmitter and the receiver. The performance of these two models was then investigated using Monte Carlo simulations. It was shown that the power attenuation parameter α in a multilayer structure is a function of effective values of dielectric properties

which in turn are functions of ϵ', σ and the thickness of all layers. Assuming known values for the thicknesses of the layers, our Adaptive Model reduced the standard deviation of the modelling error by 55% compared to that of the Fixed-Optimised Model with a constant attenuation parameter. This result is especially important for endoscopic capsule localisation since the thicknesses of the layers between the capsule and each of the receivers place on the body are unequal. We further studied the performance of our Adaptive Model in a more realistic scenario in which the thicknesses of all layers composing the medium are unknown. Our analysis showed that the thickness of the fat layer has the greatest influence on the total effective permittivity of the abdominal medium, due to the large difference in ϵ' and σ compared to those of other layers.

ACKNOWLEDGMENT

The authors would like to thank M.D., Ph.D. David Cave from the Medical School, University of Massachusetts and M.D., Ph.D. Jens Kjeldsen from the Medical School, University of Southern Denmark for providing valuable insights into challenges of capsule endoscopy navigation and localisation.

APPENDIX A. LAYER RECURSIONS FOR MULTIPLE DIELECTRIC SLABS

Defining $E_{\pm,i}$ and $E'_{\pm,i}$ as the elements of the electric field in the left and right sides of the ith interface, i.e.:

$$\begin{cases} E_{i,\pm} = E_{\pm}(z_i) \\ E'_{i,\pm} = E_{\pm}(z_i + 0^+) \end{cases}; \quad i = 1, 2, \ldots, M+1 \tag{A1}$$

$E_{\pm,i}$ and $E'_{\pm,i}$ in each interface i can be expressed as a function of $E_{\pm,i+1}$ and $E'_{\pm,i+1}$ in the next interface $i+1$ by a recursive equation [31]:

$$\begin{bmatrix} E_{i,+} \\ E_{i,-} \end{bmatrix} = \frac{1}{1+\rho_i} \begin{bmatrix} e^{j\delta_i} & \rho_i e^{-j\delta_i} \\ \rho_i e^{j\delta_i} & e^{-j\delta_i} \end{bmatrix} \begin{bmatrix} E_{i+1,+} \\ E_{i+1,-} \end{bmatrix}; \quad i = M, M-1, \ldots, 1 \tag{A2}$$

in which ρ_i and δ_i are the reflection coefficient and the phase thickness of the ith layer, respectively:

$$\rho_i = \frac{n_{i-1} - n_i}{n_{i-1} + n_i}, \quad \delta_i = \frac{\omega l_i n_i}{c_0} \tag{A3}$$

n_i and l_i are the refractive index and thickness of ith layer, and c_0 is the speed of light in vacuum. Assuming that the $(M+1)$th layer is semi-infinite, the electric field in the $(M+1)$th interface is given by:

$$\begin{bmatrix} E_{M+1,+} \\ E_{M+1,-} \end{bmatrix} = \frac{1}{1+\rho_{M+1}} \begin{bmatrix} 1 & \rho_{M+1} \\ \rho_{M+1} & 1 \end{bmatrix} \begin{bmatrix} E'_{M+1,+} \\ 0 \end{bmatrix} \tag{A4}$$

Furthermore, the electric field at each location along the z axis inside the layer i can be written as a function of E at the interface of the layer $i+1$:

$$\begin{bmatrix} E_+(z) \\ E_-(z) \end{bmatrix}_{z_i < z \le z_{i+1}} = \begin{bmatrix} e^{j\hat{\delta}_i} & 0 \\ 0 & e^{-j\hat{\delta}_i} \end{bmatrix} \begin{bmatrix} E_{i+1,+} \\ E_{i+1,-} \end{bmatrix}; \quad i = 1, 2, \ldots, M \tag{A5}$$

where:

$$\hat{\delta}_i = \frac{\omega \hat{l}_i n_i}{c_0}, \quad \hat{l}_i = z_{i+1} - z \tag{A6}$$

and for the last semi-infinite layer $M+1$:

$$\begin{bmatrix} E_+(z) \\ E_-(z) \end{bmatrix}_{z_{M+1} < z} = \begin{bmatrix} e^{j\delta_{M+1}} E'_{M+1,+} \\ 0 \end{bmatrix}; \quad \delta_{M+1} = \frac{\omega\, l_{M+1} n_b}{c_0}, \quad l_{M+1} = z - z_{M+1} \tag{A7}$$

REFERENCES

1. Than, T. D., G. Alici, H. Zhou, and W. Li, "A review of localization systems for robotic endoscopic capsules," *IEEE Transactions on Biomedical Engineering*, Vol. 59, No. 9, 2387–2399, 2012.
2. Hu, C., M. Q. Meng, and M. Mandal, "Efficient magnetic localization and orientation technique for capsule endoscopy," *IEEE 'IROS'*, 628–633, 2005.
3. Salerno, M., G. Ciuti, G. Lucarini, R. Rizzo, P. Valdastri, A. Menciassi, A. Landi, and P. Dario, "A discrete-time localization method for capsule endoscopy based on on-board magnetic sensing," *Measurement Science and Technology* Vol. 23, 015701, 2012.
4. Pahlavan, K., Y. Ye, R. Fu, and U. Khan, "Challenges in channel measurement and modeling for RF localization inside the human body," *International Journal of Embedded and Real-Time Communication Systems*, Vol. 3, No. 3, 18–37, 2012.
5. Fischer, D., R. Shreiber, G. Meron, M. Frisch, H. Jacob, A. Glukhovsky, and A. Engel, "Localization of the wireless capsule endoscope in its passage through theGI tract," *Gastrointestinal Endoscopy*, Vol. 53, AB126, 2001.
6. Fischer, D., "Capsule endoscopy: The localization system," *Gastrointestinal Endoscopy Clin., North Amer.*, Vol. 14, 25–31, 2004.
7. Abbasi, Q. H., A. Sani, A. Alomainy, and Y. Hao, "Numerical characterization and modeling of subject-specific ultrawideband body-centric radio channels and systems for healthcare applications," *IEEE Transactions on Information Technology in Biomedicine — TITB*, Vol. 16, No. 2, 221–227, 2012.
8. Fort, A., C. Desset, P. De Doncker, P. Wambacq, and L. Van Biesen, "An ultra-wideband body area propagation channel model — From statistics to implementation," *IEEE Trans. on Microwave Theory and Techniques*, Vol. 54, No. 4, 1820–1826, 2006.
9. Fort, A., J. Ryckaert, C. Desset, P. De Doncker, P. Wambacq, and L. Van Biesen, "Ultra-wideband channel model for communication around the human body," *IEEE Journal on Selected Areas in Communications*, Vol. 24, No. 4, 927–933, 2006.
10. Liu, L., R. D'Errico, L. Ouvry, P. De Doncker, and C. Oestges, "Dynamic channel modeling at 2.4 GHz for on-body area networks," *Advances in Electronics and Telecommunications*, Vol. 2, No. 4, 18–27, 2011.
11. Takada, J., T. Aoyagi, K. Takizawa, N. Katayama, H. Sawada, T. Kobayashi, K. Y. Yazdandoost, H. Li, and R. Kohno, "Static propagation and channel models in body area," *COST 2100 6th Management Committee Meeting*, Lille, France, 2008.
12. Aoyagi, T., K. Takizawa, T. Kobayashi, J. Takada, and R. Kohno, "Development of a WBAN channel model for capsule endoscopy," *Proceedings of the Antennas and Propagation Society International Symposium*, 1–4, 2009.
13. Kiourti, A., K. A. Psathas, and K. S. Nikita, "Implantable and ingestible medical devices with wireless telemetry functionalities: A review of current status and challenges C," *Wiley Bioelectromagnetics*, Vol. 35, No. 1, 1–15, 2014.
14. Basar, M. R., F. Malek, K. M. Juni, M. I. M. Saleh, M. S. Idris, and L. Mohamed, "The use of a human body model to determine the variation of path losses in the human body channel in wireless capsule endoscopy," *Progress In Electromagnetics Research*, Vol. 133, 495–513, 2013.
15. Lopez-Linares Roman, K., G. Vermeeren, A. Thielens, W. Joseph, and L. Martens, "Characterization of path loss and absorption for a wireless radio frequency link between an in-body endoscopy capsule and a receiver outside the body," *EURASIP Journal on Wireless Communications and Networking*, Vol. 21, 2014.
16. Kurup, D., W. Joseph, G. Vermeeren, and L. Martens, "Path loss model for in-body communication in homogeneous human muscle tissue," *Electronics Letters*, Vol. 45, No. 9, 453–454, 2009.
17. Xu, L. S., M. Q. H. Meng, and Y. W. Chan, "Effects of dielectric parameters of human body on radiation characteristics of ingestible wireless device at operating frequency of 430 MHz," *IEEE Transactions on Biomedical Engineering*, Vol. 56, No. 8, 2083–2094, 2009.

18. Wang, L., C. Hu, T. L. Tian, M. Li, and M. Q. H. Meng, "A novel radio propagation radiation model for location of the capsule in GI tract," *Proc. IEEE Int. Conf. Rob. Biomimetics*, 2332–2337, 2009.
19. Swar, P., K. Pahlavan, and U. Khan, "Accuracy of localization system inside human body using a fast FDTD simulation technique," *6th International Symposium on Medical Information and Communication Technology (ISMICT)*, 1–6, 2012.
20. Støa, S., R. Chavez-Santiago, and I. Balasingham, "An ultra wideband communication channel model for the human abdominal region," *GLOBECOM Workshops (GC Wkshps)*, 246–250, 2010.
21. Sayrafian-Pour, K., W.-B. Yang, J. Hagedorn, J. Terrill, and K. Y. Yazdandoost, "A statistical path loss model for medical implant communication channels," *IEEE 20th International Symposium on Personal, Indoor and Mobile Radio Communications*, 2995–2999, Sep. 13–16, 2009.
22. Nadimi, E. S. and V. Tarokh, "Bayesian source localization in networks with heterogeneous transmission medium," *Navigation*, Vol. 59, No. 3, 163–175, Washington, 2012.
23. Gabriel, C., "Compilation of the dielectric properties of body tissues at RF and microwave frequencies," Report N.AL/OE-TR-1996-0037, Occupational and Environmental Health Directorate, Radiofrequency Radiation Division, Brooks Air Force Base, Texas, USA, 1996, Available: http://www.itis.ethz.ch/itis-for-health/tissue-properties/database/dielectric-properties/.
24. Theilmann, P. T., M. A. Tassoudji, E. H. Teague, D. F. Kimball, and P. M. Asbeck, "Computationally efficient model for UWB signal attenuation due to propagation in tissue for biomedical implants," *Progress In Electromagnetics Research B*, Vol. 38, 1–22, 2012.
25. Thiel, F. and F. Seifert, "Noninvasive probing of the human body with electromagnetic pulses: Modeling of the signal path," *J. Appl. Phys.*, Vol. 105, No. 4, 044904(1–9), 2009.
26. Varotto, G. and E. M. Staderini, "A 2D simple attenuation model for EM waves in human tissues: Comparison with a FDTD 3D simulator for UWB medical radar," *IEEE International Conference on UltraWideband (ICUWB)*, Vol. 3, 1–4, 2008.
27. Pozar, D. M., *Microwave Engineering*, 4th Edition, JohnWiley & Sons, Inc., 2011.
28. Takizawa, K., H. Hagiwara, and K. Hamaguchi, "Path-loss estimation of wireless channels in capsule endoscopy from X-ray CT images," *33rd Annual International Conference of the IEEE EMBS*, 2242–2245, Boston, Massachusetts, USA, Aug. 30–Sep. 3, 2011.
29. Zhao, J., D. Liao, and B. P. McMahon, "Functional luminal imaging probe geometric and histomorphologic analysis of abdominal wall wound induced by different trocars in pigs," *Surg. Endosc.*, Vol. 23, 1004–1012, 2009.
30. Cheng, L., C. Wu, Y. Zhang, H. Wu, M. Li, and C. Maple, "A survey of localization in wireless sensor network," *Int. J. Distrib. Sens. Netw.*, Vol. 2012, 1–12, 2012.
31. Orfanidis, S. J., *Electromagnetic Waves and Antennas*, Online Book, 1999.